POLITECNICO DI TORINO
Repository ISTITUZIONALE

Study of microring nonlinearities in silicon photonics for neuromorphic computing

Original
Study of microring nonlinearities in silicon photonics for neuromorphic computing / Salpietro, S., Novarese, M., Rimoldi, C., Gioannini, M.. - 13371:(2025), pp. 1-7. (SPIE Photonics West - OPTO San Francisco (USA) 25-30 January 2025) [10.1117/12.3040062].

Availability:
This version is available at: 11583/2998718 since: 2025-04-01T13:21:21Z

Publisher:
SPIE

Published
DOI:10.1117/12.3040062

Terms of use:

This article is made available under terms and conditions as specified in the corresponding bibliographic description in the repository

Publisher copyright

(Article begins on next page)

21 June 2026

Study of Microring Nonlinearities in Silicon Photonics for Neuromorphic Computing

Salvatore Salpietro[a], Marco Novarese[a], Cristina Rimoldi[a], and Mariangela Gioannini[a]

[a]Dipartimento di Elettronica e Telecomunicazioni, Politecnico di Torino, corso Duca degli Abruzzi 24, Torino, IT-10129 Italy

ABSTRACT

We analyze a theoretical and experimental reservoir computing architecture based on an add-drop silicon microring resonator. We test it with different datasets, including the recognition of flowers from the IRIS dataset.The information is transferred to the ring by means of a high power (>10 mW) pump signal which generates nonlinearities affecting a low-power continuous wave signal acting as a probe. The experimental setup was also simulated employing a time domain model [1] of the non-linear response of the ring to assess the physical limit of the pump power.

Keywords: reservoir computing, silicon micro-ring resonators, silicon non-linearities, pump-probe setup, silicon photonics platform, Iris dataset, Shockley-Read-Hall, free carrier absorption, two-photon absorption, carrier lifetime, photonic neural networks.

1. INTRODUCTION

The objective of our work is to analyze how the nonlinear properties of optical micro-ring resonators, integrated into a silicon photonics platform, can be exploited to build up a neural network capable of solving complex tasks using the reservoir computing technique, as demonstrated for the first time in [2]. We used a silicon micro-ring resonator in an add-drop configuration (with a quality factor of approximately 13000). This model is applied to the simulation of the micro-ring in the recognition of the Iris flower dataset. This problem was also addressed experimentally by setting up a pump-probe setup, which is shown in Figure 1. A high-power pump laser was used to induce nonlinear effects in the resonator, while a low-power probe laser, tuned to an adjacent resonance, was employed to monitor these effects. The laser pump was modulated using a Mach-Zehnder modulator with a waveform, that is the encoded input. For the Iris dataset, the input was encoded with the petal and sepal length and width measurements, preprocessed by applying a mask. The probe response at the output of the micro-ring is sampled and the data are used to train and test the neural network, achieving classification accuracies comparable to those obtained in simulations and exceeding 90%.

In microring resonators, the nonlinear effects are of fundamental importance because they modify the optical response of the ring, especially at high powers. The main nonlinear effects are: two-photon absorption (TPA) and the thermo-optic effects. Two-photon absorption occurs when the combined energy of two photons is sufficient to excite an electron from the valence band to the conduction band. This excitation generates free carriers in both the conduction and valence bands, inducing the nonlinear phenomena of free-carrier absorption (FCA) and free-carrier dispersion (FCD). FCA refers to the absorption of a photon by the newly generated free carriers, exciting them to a higher energy state. This process affects the imaginary part of the refractive index. On the other hand, FCD modifies the real part of the refractive index due to the presence of these free carriers.

The thermo-optic effect arises from thermalization and recombination through Shockley-Read-Hall (SRH) processes, which generate heat (self-heating). This increase in temperature alters the refractive index of the silicon waveguide.

The thermo-optic effect causes a resonance shift towards longer wavelengths, while FCD shifts the resonance towards shorter wavelengths.

TPA and FCA rise the overall optical loss reducing the quality factor of the resonator. Therefore, the total modal

Further author information: (Send correspondence to M.N.)
M.N.: E-mail: marco.novarese@polito.it

Silicon Photonics XX, edited by Graham T. Reed, Jonathan Bradley,
Proc. of SPIE Vol. 13371, 133710L · © 2025 SPIE
0277-786X · doi: 10.1117/12.3040062

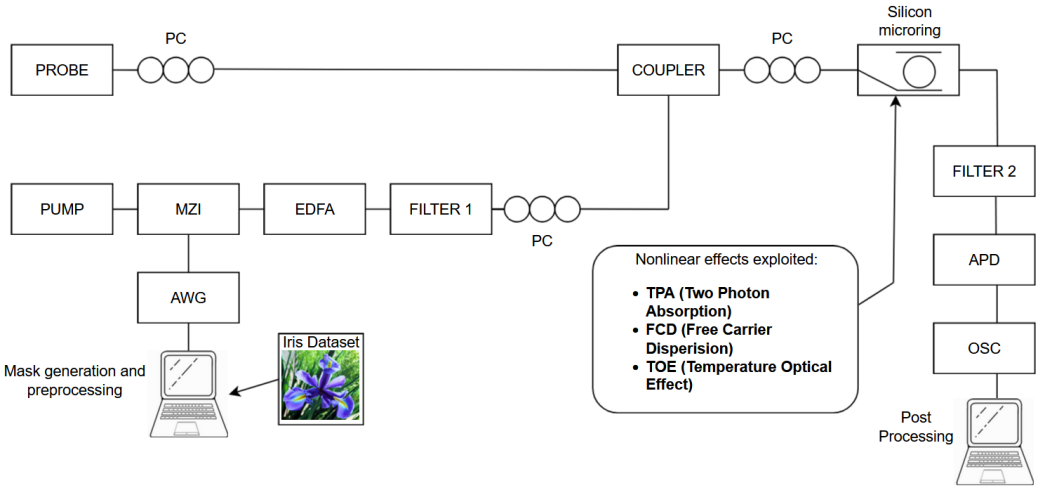

Figure 1: Experimental setup for the pump-probe measurement with the silicon photonics microring resonator. The configuration includes: Probe laser source, Pump laser source, Mach-Zehnder Interferometer (MZI), Erbium-Doped Fiber Amplifier (EDFA), various filters (FILTER1 and FILTER 2), coupler, polarization controllers (PC), Avalanche Photodiode (APD) and Oscilloscope (OSC) with a computer for mask generation, preprocessing and post-processing.

loss of the optical field includes linear losses (α_0), bending losses (α_{rad}), and nonlinear losses (due to TPA, FCA, and cross two-photon absorption (XTPA).
For the pump field, these effective losses are expressed as:

$$\alpha_{\text{eff,pump}} = \alpha_0 + \alpha_{\text{rad}} + \frac{\alpha_{\text{TPA}} P_{\text{c,pump}}}{A_{\text{eff}}} + \frac{2\alpha_{\text{TPA}} P_{\text{c,probe}}}{A_{\text{eff}}} + \Gamma \Delta\alpha_{\text{FCA}} \tag{1}$$

where Γ represents the optical confinement factor, $P_{\text{c,pump}}$ represents the circulating pump power, A_{eff} is the effective area, α_{TPA} is the TPA coefficient, and $\Delta\alpha_{\text{FCA}}$ accounts for free-carrier absorption losses. The FCA losses depend on the electron and hole densities (n_e and p_e respectively) and are described by the empirical expression provided in [3]:

$$\Delta\alpha_{\text{FCA}}(n_e, p_e) = 8.88 \cdot 10^{-21} n_e^{1.167} + 5.84 \cdot 10^{-20} p_e^{1.109} \tag{2}$$

The same equation applies to the probe signal, replacing $P_{\text{c,pump}}$ with $P_{\text{c,probe}}$ and vice versa.
Thus, the formula that accounts for the electric field loss per round trip in the resonator is:

$$a_{\text{pump}} = e^{-\left(\alpha_{\text{eff,pump}} \frac{L}{2}\right)} \tag{3}$$

where L is the is the ring path length.
The total variation in the refractive index is mainly due to the contributions from FCD, thermal effects and Kerr effect.
The total refractive index variation caused by the pump is expressed as:

$$dn_{\text{eff,pump}} = dn_{\text{eff,FCA}} + dn_{\text{eff,T}} + dn_{\text{eff,Kerr,pump}} \tag{4}$$

with [3]:

$$dn_{\text{eff,FCA}} = -\Gamma \left(5.4 \cdot 10^{-22} n_e^{1.011} + 1.53 \cdot 10^{-18} p_e^{0.838}\right) \tag{5}$$

and:

$$dn_{\text{eff,T}} = \Gamma \frac{dn_{\text{Si}}}{dT} \Delta T_{\text{tot}} \tag{6}$$

$$dn_{\text{eff,Kerr,pump}} = \Gamma n_2 \left(\frac{P_{\text{c,pump}}}{A_{\text{eff}}} + 2\frac{P_{\text{c,probe}}}{A_{\text{eff}}}\right) \tag{7}$$

where $\frac{dn_{\mathrm{Si}}}{dT}$ is the thermo-optic coefficient of silicon, and $n_2 = 4.4 \cdot 10^{-18}\,[\mathrm{m}^2/\mathrm{W}]$ is the Kerr coefficient for silicon. For the probe field, the equation remains the same but with the standard interchange of terms corresponding to the pump and probe fields.
The dynamic behavior of the circulating field in the microring resonator, which depends on the total losses and total refractive index, is described by the equation 8:

$$\begin{aligned}\frac{\partial E_{c,i}}{\partial t} &= \left(\left(-\kappa_i \cdot \sqrt{1-\eta^2} \cdot \frac{1}{t_i^2 \cdot a_i(t)}\right) E_{\mathrm{bus},i} + E_{c,i}(t)\left(\frac{1}{t_i^2 \cdot a_i(t)} - 1\right)\right)/\tau_g + \\ &+ \left(-i \cdot \left(\frac{2\pi c_0}{\lambda_i} \cdot \Delta n_{\mathrm{eff},i}(t) \cdot \frac{L}{c_0} + \omega_{2,i} \cdot n_g \cdot \frac{L}{c_0}\right) E_{c,i}(t)\right)/\tau_g, \end{aligned} \tag{8}$$

where i = pump, probe.
The key terms in Equation 8 are explained below:

- κ_i: is the ring coupling coefficient.
- η^2: accounts for the coupling losses.
- $t_i^2 = 1 - k_i^2 - \eta^2$.
- $E_{\mathrm{bus},i}$: is the input field.
- $\tau_g = \frac{L \cdot n_g}{c}$

The variation of free electron and hole densities, induced by the circulating power and Shockley-Read-Hall (SRH) recombination, are described by Equations 9 and 10:

$$\frac{dp_e}{dt} = G - \frac{1}{\tau_{p0}}\left(\frac{(p_0 + p_1 + p_e)(p_e - n_e)}{N_f} + \frac{p_e p_1}{p_e + p_0}\right), \tag{9}$$

$$\frac{dn_e}{dt} = G - \frac{1}{\tau_{n0}}\left(\frac{(n_0 + n_1 + n_e)(n_e - p_e)}{N_f} + \frac{n_e n_1}{n_e + n_0}\right), \tag{10}$$

where:

- n_0, p_0 and n_1, p_1 are the electron and hole concentrations under equilibrium conditions,
- N_f is the trap density,
- τ_{n0} and τ_{p0} are the capture time in the trap of electrons and holes respectively.

The first term on the right-hand side represents the generation rate G, while the second term corresponds to the SRH recombination. The total carrier generation rate for the pump, G_{pump}, is defined as the sum of the contributions from TPA and XTPA:

$$G_{\mathrm{pump}} = G_{\mathrm{pump,TPA}} + G_{\mathrm{pump,XTPA}} \tag{11}$$

where contributions are defined as:

$$G_{\mathrm{pump,TPA}} = \frac{\alpha_{\mathrm{TPA}} P_{\mathrm{c,pump}}^2}{2\frac{hc}{\lambda_{\mathrm{pump}}} A_{\mathrm{eff}}} \tag{12}$$

$$G_{\mathrm{pump,XTPA}} = \frac{2\alpha_{\mathrm{TPA}} P_{\mathrm{c,pump}} P_{\mathrm{c,probe}}}{\frac{hc}{\lambda_{\mathrm{pump}}} A_{\mathrm{eff}}} \tag{13}$$

where:

- $P_{\mathrm{c,probe}}$ is the circulating power of the probe,

- λ_{pump} is the pump wavelength,

Furthermore, the relaxation of free carriers, triggered by FCA, leads to an increase in the system's temperature. The temperature dynamic can be described by the equation 14:

$$\frac{d\Delta T_i(t)}{dt} = -\frac{\Delta T_i(t)}{\tau_{\text{th},i}} + \frac{P_{\text{abs},pump}(t) + P_{\text{abs},probe}(t)}{C_i}, \tag{14}$$

for pump and probe fields with $i = 0, 1, 2, 3$ referring to the four nodes of the equivalent thermal circuit of the ring. Here, $\tau_{\text{th},i} = Z_{T,i}C_i$ is the thermal time constant associated with a distinct thermal node of the equivalent thermal model of the microring, and P_{abs} denotes the total absorbed optical power.

2. RESULTS

We experimentally measured the temporal evolution of the pump input (before the micro-ring) and probe output (after the micro-ring) signals while varying the number of virtual nodes (N_v), samplerate (S) and mean input power (P_m). Figure 2 illustrates the temporal evolution of these two signals for a single flower from the IRIS dataset with $S = 10\,\text{MSps}$, $N_v = 50$ and $P_m = 4.8$ dBm.

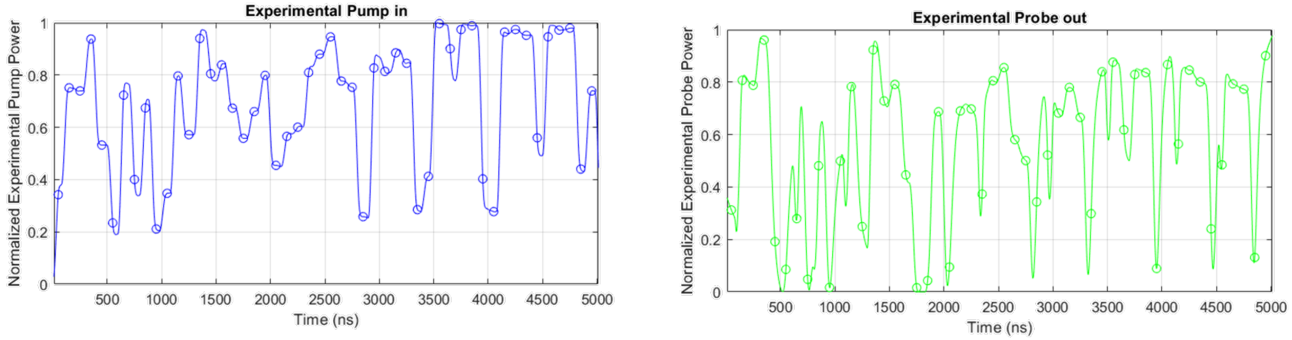

(a) (b)

Figure 2: (a) Temporal evolution of the pump input signal before the microring for a single flower. (b) Temporal evolution of the probe output signal after the microring for a single flower.

As shown in Figure 3, sampling the output probe power results in a higher classification accuracy (97.73% at 10 MSps, meaning that 97.73% of the flowers in the IRIS dataset were correctly classified) compared to sampling the input pump power (84.1%). This demonstrates that the non-linear responce of the probe to the excitation pump enhances the task resolution with greater precision.
These results at 10 MSps validate our setup by comparing it with those reported in [2].
Furthermore, we performed a simulation-based analysis to investigate the impact of the average input power (P_m) on system performance.
In Figure 4, four graphs obtained through simulations are shown, illustrating the various physical phenomena involved for the classification of the IRIS dataset. The graphs highlight the transmission coefficient, electron and hole density, and temperature variation for three average pump power levels: 2, 4, and 8 dBm, with a samplerate of 30 MSps and 50 virtual nodes. In the graph of the transmission coefficient evaluated at the probe wavelength, at high pump powers, time frames are created where the coefficient reaches very high values. These are circled in red, as seen at 8 dBm. This indicates that, in these regions, the microring is less efficient at transferring information from the pump to the probe. When the wavelength of the injected signal is no longer aligned with the resonance of the microring, the circulating power inside the microring decreases, along with the nonlinear effects.
This behavior can be better understood by observing Figure 5.
In this figure, it can be seen that when the electron density rapidly decreases, the shift of the resonance wavelength due to free carrier dispersion quickly cancels out, while the shift due to the temperature decreases more slowly.

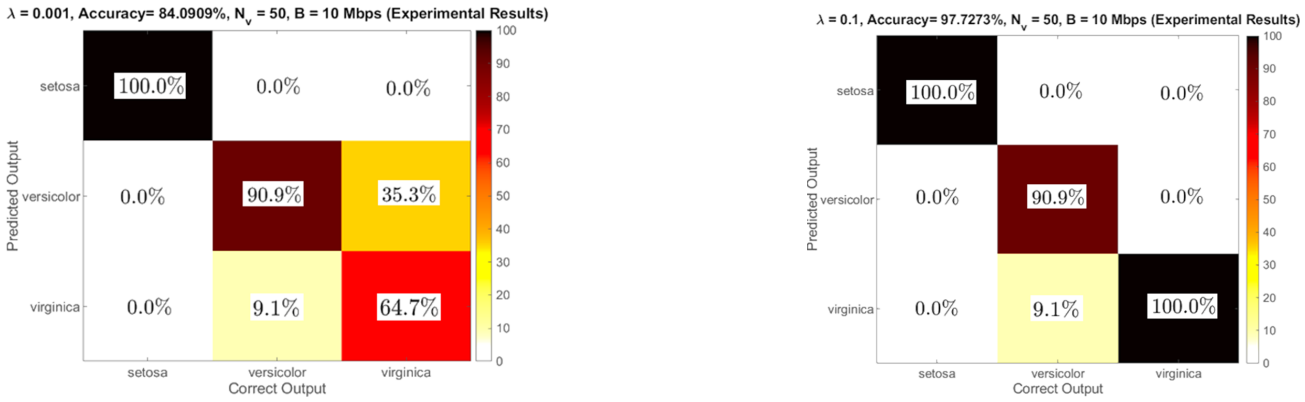

(a) (b)

Figure 3: (a) Error map obtained from sampling the input pump signal before the microring. (b) Error map obtained from sampling the output probe signal after the microring.

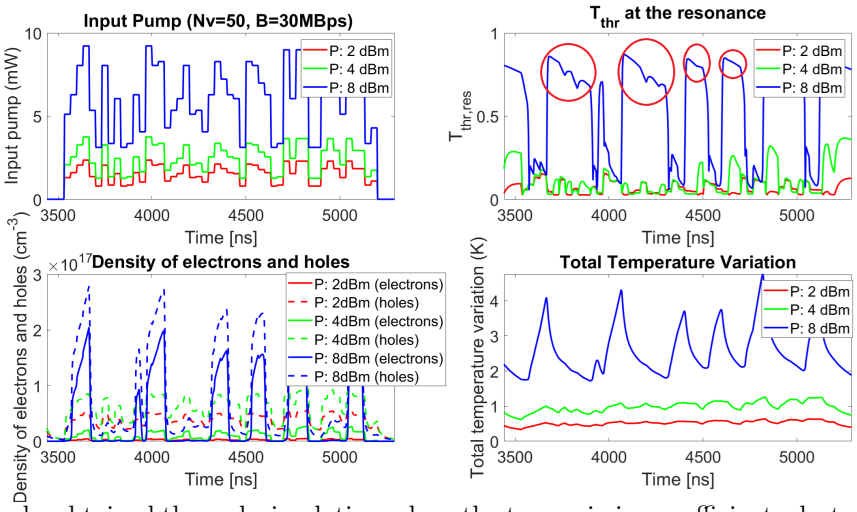

Figure 4: These graphs obtained through simulations show the transmission coefficient, electron and hole density, and temperature variation for three average pump power levels: 2, 4, and 8 dBm, with a samplerate of 30 MSps and 50 virtual nodes.

This difference in speed drives the microring quickly out of resonance. Additionally, the higher the pump power, the longer it will take for the system to return to resonance, as the cooling process will take more time. This explains why at high power levels, the out-of-resonance time frames are wider and persist for longer.

At lower power levels, this phenomenon is reduced because the temperature effect is less significant, allowing the pump to transfer information to the probe more accurately. However, at very low power levels, the amount of nonlinearities caused by the pump are negligible, therefore the transmission coefficient varies so little that the pump cannot effectively transfer information to the probe.

As illustrated in Figure 6, the accuracy initially improves as the pump power increases, reaching its maximum value within the pump power range of 0 dBm to 10 dBm, after which it begins to decrease.

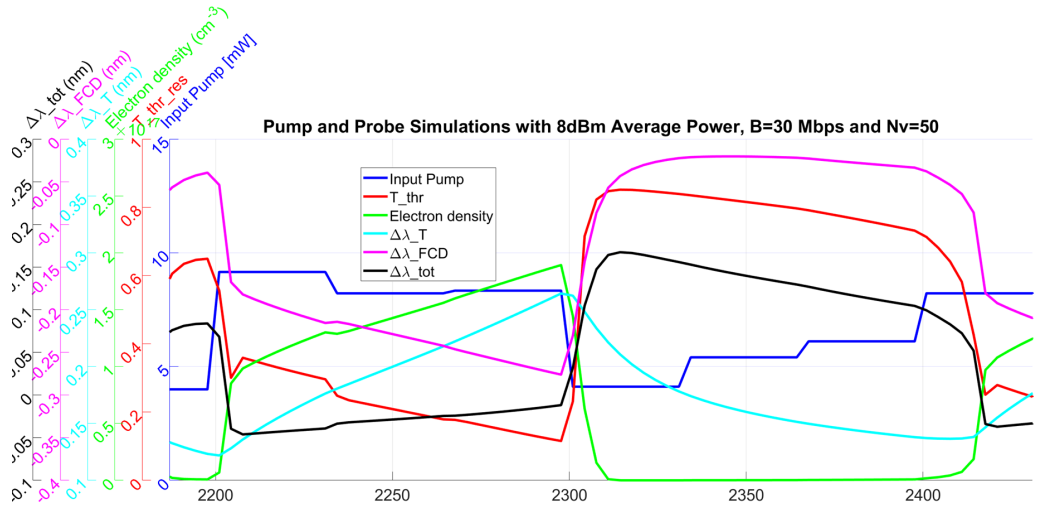

Figure 5: Time evolution of the input pump power (blue line), the transmission coefficient T_{thr} at resonance (red line), the electron density (green line), the resonance wavelength shift due to temperature variation $\Delta\lambda_T$ (magenta line), the shift due to FCD $\Delta\lambda_{\text{FCD}}$ (cyan line), and the total wavelength shift $\Delta\lambda_{\text{tot}}$ (black line).

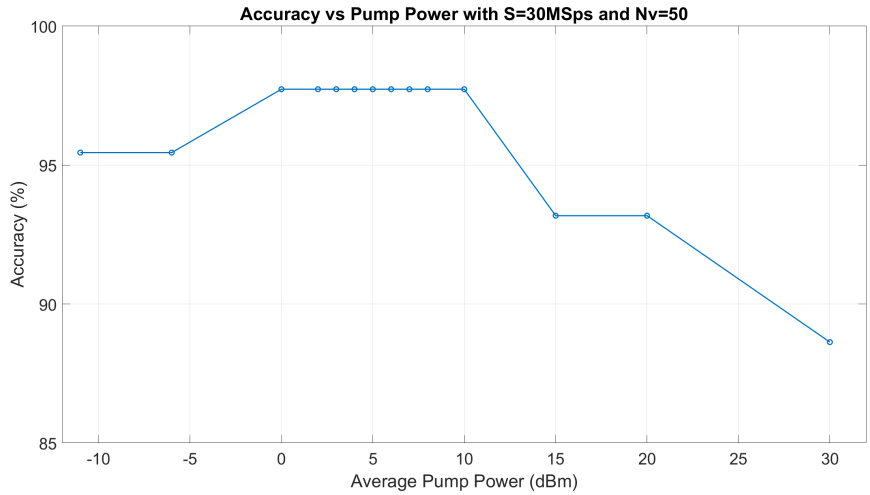

Figure 6: Accuracy as a function of average pump power for a sampling rate of 30 MSps and $N_v = 50$.

3. CONCLUSIONS

We investigated how the nonlinearities induced by FCD, TPA, and self-heating in a silicon microring resonator at the through port significantly improve the classification accuracy of a neural network based on reservoir computing. Experimental results showed that sampling the input power without passing through the microring leads to significantly lower accuracies (84.1% for a samplerate of 10 MSps) compared to the 97.73% achieved by sampling the output probe signal at 10 MSps. This demonstrates that the nonlinearities introduced by the microring are essential for optimal dataset classification. Simulation results also showed that the classification accuracy decreases at both very low and very high power levels. By the analysis of these results we could observed that the self-heating and slow thermal transient is the main factor limiting the maximum pump power to be injected.

Our future work will focus on reservoir computing platforms employing other silicon ring structures with smaller carrier lifetimes (<1 ns), as these could enable operation at samplerates exceeding 1 GHz, further enhancing the performance and scalability of this reservoir computing network.

References

[1] Novarese, M., Romero Garcia, S., Cucco, S., Adams, D., Bovington, J., and Gioannini, M., "Study of nonlinear effects and self-heating in a silicon microring resonator including a shockley-read-hall model for carrier recombination," *Optics Express* **30**(9), 14341–14357 (2022).

[2] Borghi, M., Biasi, S., and Pavesi, L., "Reservoir computing based on a silicon microring and time multiplexing for binary and analog operations," *Scientific Reports* **11**, Article 99525 (2025).

[3] Nedeljkovic, M., Soref, R., and Mashanovich, G. Z., "Free-carrier electrorefraction and electroabsorption modulation predictions for silicon over the 1–14-m infrared wavelength range," *IEEE Photonics Journal* **3**(6), 1171–1180 (2011).